Chinese Journal of Chemical Engineering 67 (2024) 117–125

Contents lists available at ScienceDirect

Chinese Journal of Chemical Engineering

journal homepage: www.elsevier.com/locate/CJChE

Full Length Article

Hydrodynamic analysis of carbon nanotube clusters in distributor-less conical fluidized beds with step-by-step scaling

Tianle Zhang [1], Wenjuan Bai [1,*], Qianpeng Dong [1], Dianming Chu [1], Lianlian Wang [2], Yan He [1,*]

[1] *Shandong Engineering Laboratory for Preparation and Application of High-performance Carbon-Materials, College of Electromechanical Engineering, Qingdao University of Science and Technology, Qingdao 266061, China*

[2] *Shandong Dazhan Nano Materials Co., Ltd., Binzhou 256220, China*

ARTICLE INFO

Article history:
Received 7 July 2023
Received in revised form
27 November 2023
Accepted 5 December 2023
Available online 20 December 2023

Keywords:
Carbon nanotubes
Fluidized bed
Multiphase flow
Scale-up
Multiscale

ABSTRACT

As a high-performance material with great application potential, the application of carbon nanotubes has been limited by their production volume. A distributor-less conical fluidized bed is the main equipment used in the industrial production of carbon nanotubes. To improve the production volume and product quality of carbon nanotubes, the study of fluidized-bed-diameter scaling is important. Three different diameters of distributor-less conical fluidized beds were established, and then the particle behavior and bubble characteristics of carbon nanotube clusters at these bed diameters were investigated. Time-series and wavelet analysis methods were used to analyze the pressure-fluctuation signals inside the fluidized beds. Results showed that the distributor-less design caused the airflow to break through the middle of the bed, which did not change with the change in bed diameter. The powder-bridging phenomenon of carbon nanotube clusters in a 100-mm-diameter fluidized bed was related to the special microstructure of carbon nanotube clusters. The frequency of pressure fluctuations in the bed decreased nonlinearly with increasing bed diameter. This study can guide the design and scale-up of distributor-less conical fluidized beds, especially for the scale-up of carbon nanotube production equipment, which can contribute to the improvement of carbon nanotubes' capacity and quality in industrial production.

1. Introduction

Fluidized beds have gained great popularity as well-established production equipments since first being put into commercial use in 1920. Compared to fixed bed reactors, fluidized bed reactors offer advantages such as good particle mixing and greatly increased gas–solid contact area in catalytic reactions containing solid catalysts [1–4]. In addition to promoting mass transfer, gas–solid mixing also improves the heat transfer between the particles, gas, and the reactor wall or heat exchange tube, allowing a constant temperature and pressure to be maintained inside the reactor [5]. With fluidized bed reactors, unique processes can be used to produce gasoline, perform ore calcination, coal and biomass combustion, and olefin polymerization, and produce biosynthetic methane, all of which are widely used in the chemical, metallurgical, environmental, and pharmaceutical industries [6–8].

Carbon nanotubes are seamless cylinders formed by the convolution of one or more layers of graphite and have good mechanical, electrical and thermal properties [9]. Furthermore, they can be widely used in various fields, *e.g.*, agriculture, microelectronics, quantum technology, bio-detection, environmental protection and energy storage [10–15]. However, carbon nanotubes are currently not available for large-scale applications due to production costs and production volume limitations. Solving the problem of low-cost, large-scale production of carbon nanotubes is the top priority for carbon nanotube applications. Fluidized bed reactors can provide good gas–solid contact area and growth space, and combined with the chemical-vapor deposition method in preparing carbon nanotubes—currently provide the best solution to increase the production volume of carbon nanotubes [16]. The focus in the bulk preparation of carbon nanotubes must be on the fluidization of the carbon nanotube cluster particles, which includes the interaction between the particles and the gas, between the particles, and between the particles and the reactor walls [17].

Carbon nanotubes tend to clog the distributor and cause dead zones during their growth because they are sticky nanoclusters

* Corresponding author.
E-mail addresses: bwj@qust.edu.cn (W. Bai), heyan@qust.edu.cn (Y. He).

https://doi.org/10.1016/j.cjche.2023.12.001
1004-9541/

with a three-dimensional mesh structure of attachments. Furthermore, because the preparation of carbon nanotubes is performed at high temperatures (generally >600 °C), long-term continuous use will lead to clogging, sintering, and fatigue fracture of the distributor. Accordingly, we proposed a distributor-less conical fluidized bed in the previous stage of our research [18]. In this particular fluidized bed, the characteristics of gas–solid two-phase flow are not only affected by various factors, *e.g.*, the density difference between the two phases of gas–carbon nanotube clusters and cluster characteristics but also change with the change in fluidized bed diameter. Moreover, the performance of the fluidized bed has been significantly influenced by the size of the bed diameter, which is the focus and difficulty of fluidization research. Over the past century, the scaled-up design methods for fluidized beds have changed from simple scale-up and Edisonian unit experiments to advanced modeling, cold fluidization tests, and pilot plants associated with machine learning [19]. It is necessary to study the hydrodynamic properties of the bed in detail to improve the scale-up of fluidized bed reactors. Therefore, to achieve the development of carbon nanotube fluidization technology and the mass production of carbon nanotubes, it is important to study the fluidization behavior of a step-by-step scale-up of a distributor-less conical fluidized bed and the flow structure of carbon nanotubes within it through experimental observations and data analysis [20].

In this paper, mass-transfer characteristic tests of carbon nanotube cluster fluidization were conducted in three distributor-less conical fluidized beds with a step-by-step scale-up of bed size. These tests facilitated the investigation of the problems encountered in the scale-up process of the distributor-less conical fluidized bed and allowed us to gain experience for the design and scale-up of the proposed distributor-less conical fluidized bed.

2. Experimental

Experiments were performed in three cold conical fluidized beds without distributors, and polymethyl methacrylate was used as the experimental setup material. As shown in Fig. 1, the fluidized beds have diameters of 50, 100 and 300 mm, with similar geometries. In addition, as shown in Fig. 2, each is divided into an upper cone, a cylinder, and an expansion section. The fluidization of large particles is ensured by the high gas velocity of the lower cone. The presence of the upper expansion section reduces the gas velocity to prevent the fine particles it carries from being blown out. To further stop the fine particles from spilling out with the gas, the baghouse is set at the top of the expansion section.

Carbon nanotube clusters can form a three-dimensional mesh structure in the microscopic state owing to their long one-

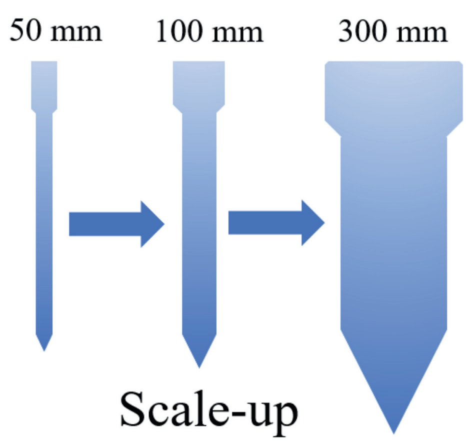

Fig. 1. Schematic diagram of fluidized bed step-by-step scaling.

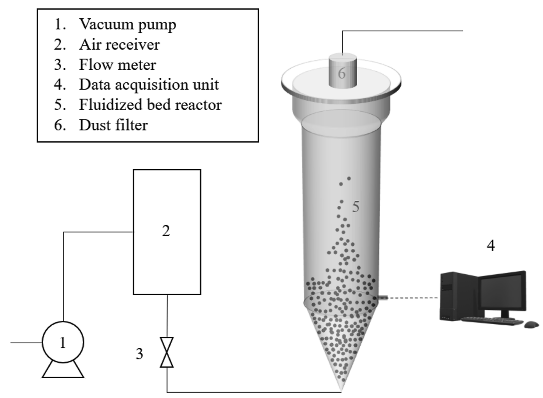

Fig. 2. Schematic of experimental apparatus.

dimensional tubular morphology and high intermolecular forces. This special structure makes the length of the fluidization time of carbon nanotube clusters affect the fluidization characteristics of the particles. In our previous work, the minimum fluidization velocity of carbon nanotube clusters was measured to be 0.04 $m \cdot s^{-1}$ by the bed expansion curve [9]. Therefore, the gas velocity was first increased above the minimum fluidization velocity (0.04 $m \cdot s^{-1}$) and completely fluidized for 10 min before the experiment to break the three-dimensional mesh structure of carbon nanotube clusters and reduce its effect on fluidization. For the experiments, the air was first compressed by a compressor into a storage tank and then dispatched through a valve control so that the velocity of the discharged gas was uniform and stable. An airflow meter with an accuracy of 4% was used to record the flow rate of the discharged gas. The gas entered the conical fluidized bed from the bottom. Pressure fluctuations between the interior of the conical fluidized bed and the ambient atmosphere were measured using a differential pressure transmitter with sampling points located at the radial center of a cylindrical section of the bed, above the static bed, and at the other end in the air environment.

A gas valve was used to control the gas velocity during fluidization, the measurement was repeated three times for each data point, and the measured data were recorded as gauge pressure, with the other port of the sensor connected to the atmosphere. Data were sampled at 200 Hz for 50- and 100-mm-diameter beds and at 400 Hz for 300-mm-diameter beds, with a continuous sampling time of 3 min.

A Testo 510i differential-pressure-measuring instrument (Testo, Germany) was used to monitor and collect the pressure drop in the bed. The measurement range was 0–15 kPa with a measurement accuracy of ±5 Pa (0–100 Pa) ± (20 Pa + 1.5% measured value) (1–15 kPa), with a resolution of 1 Pa. A CYG 1219 piezoresistive differential pressure transmitter with a range of 0–10 kPa and an accuracy of ±0.5% full scan was used to monitor pressure fluctuations. Furthermore, a USB-6002 data acquisition module was used to collect pressure fluctuation data. The measurements were recorded as gauge pressure with one port of the sensor plugged into the bed and the other port connected to the atmosphere.

Air at room temperature was used as the fluidization medium, and agglomerated multi-walled carbon nanotubes were used as the bed material. Table 1 lists the physical properties of the particles, whereas Table 2 shows the particle-size distribution.

3. Signal Processing and Analysis Methods

Pressure fluctuation signals in fluidized beds are reliable, easy to measure, highly accurate, and inexpensive and have a very important place in the study of flow characteristics in fluidized

Table 1
Experimental particle property materials

Material	Equivalent diameter d_p/mm	True density ρ_t/g·cm^{-3}	Particle porosity ε/%
MWCNT	0.78	1.51	85.468

Table 2
Particle size classification of MWCNT

Mesh size/mm	Percentage of sieve residue/%	Cumulative percentage retained/%	Percentage passing/%
2.360	0.069	0.069	99.931
1.700	0.047	0.116	99.884
1.400	0.225	0.341	99.659
1.180	0.120	0.461	99.539
1.000	2.364	2.825	97.175
0.880	2.550	5.375	94.625
0.830	5.605	10.980	89.020
0.550	11.057	22.037	77.963
0.250	65.259	87.296	12.704
0.115	12.552	99.848	0.152
Sieve bottom	0.151	99.999	0.001

beds [21]. The generation of pressure fluctuations is associated with a variety of factors, including the composition of bubble motion, bed oscillations, and pressure waves at other sites [22]. Van Ommen *et al.* [23] concluded that absolute pressure fluctuations (*i.e.*, the pressure measured at one location) reflect both local and global fluidization phenomena, but global fluidization phenomena, *i.e.*, phenomena that can be measured everywhere in the bed, such as bubble eruptions on the bed surface, have the greatest impact. Therefore, the analysis of the pressure-fluctuation signal allows us to obtain important characteristics such as the flow characteristics and bubble behavior of the particles in the fluidized bed.

3.1. Time-series analysis

The most widely used method in time-domain analysis is to determine the magnitude of pressure fluctuations, expressed as standard deviation. In fluidized beds, this method makes it possible to determine the minimum fluidization velocity [24].

Bed pressure fluctuations are represented as a time series of data points $x(n)$, where $n = 1, 2, 3, \cdots, N$; N is the total number of data points, and the sampling frequency is fs.

Pressure fluctuations are expressed as standard deviations [25]:

$$\sigma = \sqrt{\frac{1}{N-1}\sum_{n=1}^{N}(x(n)-\bar{x})^2} \tag{1}$$

where $\bar{x}$ is the average pressure.

Skewness (S) is a numerical characteristic of the degree of asymmetry in the distribution of statistical data. The equation is [26]:

$$S = \frac{1}{N\sigma^3}\sum_{n=1}^{N}(x(n)-\bar{x})^3 \tag{2}$$

The skewness of the normal distribution is 0. When $S > 0$ and $S < 0$, the distribution is skewed to the right or left, respectively.

The flatness or peak in the data distribution is called kurtosis (K) and is calculated as follows:

$$K = \frac{1}{N\sigma^4}\sum_{n=1}^{N}(x(n)-\bar{x})^4 \tag{3}$$

The kurtosis of the normal distribution is 3, and the kurtosis of the uniform distribution is 1.8. For intermittent systems, the flatness can also be considered as the ratio of the time spent in the stationary condition to the time spent in the active condition [27].

3.2. Wavelet analysis

The pressure-fluctuation signals measured from within the fluidized bed are complex and include components at multiple scales. Wanting to quantitatively analyze the dominant behavior of carbon nanotube clusters during fluidization, the pressure-fluctuation signals during fluidization can be decomposed to extract the energy shares of their individual scale structures [9,28–30]. Wavelet analysis is a signal-processing method with the advantages of multi-resolution and multi-basis functions [31] and is widely used in the analysis of fluidized bed pressure-fluctuation signals [32,33]. Bai *et al.* [34] successfully analyzed the contribution of the sub-signal to the total energy of the structure using wavelet analysis of the signal. The wavelet transform of the time series signal X is expressed as follows:

$$W_f(a,b) = \frac{1}{\sqrt{|a|}}\int_{-\infty}^{+\infty} x(t)\varphi^*_{a,b}\left(\frac{t-b}{a}\right)dt \tag{4}$$

where $W_f(a,b)$ is the wavelet coefficient; $\varphi^*_{a,b}(t)$ denotes the wavelet basis function; a and b are the expansion factor and translation factor, respectively, which range from $-\infty$ to $+\infty$, and $a \neq 0$.

The original signal will be decomposed into different levels by the discrete wavelet transform. The decomposition process is performed several times until the signal reaches the desired decomposition level J [35]. According to the theory of multiscale signal decomposition [33], the components with different resolutions represent the signal characteristics at different scales. For a continuous signal $X(t)$, the orthogonal wavelet level is approximated as follows:

$$X(t) = A_j(t) + \sum_{j=1}^{J} D_j(t) \tag{5}$$

$$A_{j+1}(t)=\sum_k h(k-2t)A_j(t) \tag{6}$$

$$D_{j+1}(t)=\sum_k g(k-2t)D_j(t) \tag{7}$$

The coefficients of the low-pass and high-pass filters calculated from the basic wavelet and scale functions are $h(k-2t)$ and $g(k-2t)$, respectively.

Third-order Daubechs wavelets (db3) can be used to analyze the signal. In this study, the multiscale signal of pressure fluctuations measured in a distributor-less conical fluidized bed was calculated using db3. According to the Nyquist sampling theorem, the sampling frequency is twice the maximum frequency of the signal to avoid the loss of useful flow information [36]. Here, a sampling frequency of 400 Hz allows the measurement of signals in the range of 0–400 Hz. Fig. 3 shows the corresponding frequency band for each sub-signal in the eight-level decomposition. Moreover, the energy of the signal is usually described by the wavelet coefficients, and the sum of the squares of the wavelet coefficients is equal to the energy of the sub-signal. Thus, the energy of the detailed signal, $D_j(t)$, can be expressed by Eq. (8) [32]:

$$E_D^j=\sum_{t=1}^{n}\left|D_j(t)\right|^2 \tag{8}$$

Calculate the total energy of the detailed signal for different levels of J and the approximate signal for level J [37]:

$$E=E_A^J+\sum_{j=1}^{J}E_D^j \tag{9}$$

4. Results and Discussion

4.1. Standard deviation of pressure fluctuations

The source of pressure fluctuations is mainly generated by the collisional oscillations of the carbon nanotube clusters with the gas stream. Fig. 4 shows the standard deviations (D_s) and data (D_d) of pressure fluctuations for three different diameters of conical fluidized beds without distributors. The pressure fluctuations for the three different diameters of the fluidized bed are represented by 50, 100 and 300 mm in the figure. The pressure fluctuations for all three fluidized beds range from 12.5 to 22.5 Pa and show different trends with increasing surface gas velocity.

Fig. 4(a) shows the standard deviation of pressure fluctuations in a 50-mm-tube-diameter fluidized bed. The pressure fluctuation decreases slowly as the surface gas velocity increases. When the gas velocity is low, the bed is not completely fluidized and the gas stream breaks through along the gap in the middle of the bed. As the gas velocity increases, it can be observed that the gas breaks up as large bubbles on the surface of the bed, driving the carbon nanotube clusters in the center of the bed upward. At this time, the collision between the gas flow and the particles is more intense,

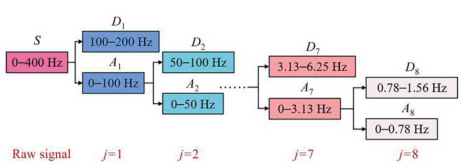

Fig. 3. The decomposition map and wavelet transform of the main signal are processed with a sampling frequency of 400 Hz.

and the pressure fluctuation is larger. When the gas velocity increases further, the bed enters into a fully fluidized state, and the large bubbles brought by the breakthrough in the middle of the gas flow turn into small bubbles uniformly and densely on the whole bed surface; the gas oscillation weakens and the amplitude of pressure fluctuation decreases. When the gas velocity exceeds 0.05 $m\cdot s^{-1}$, the fluidization of the bed gradually becomes strong, and the amplitude of pressure fluctuation starts to rise with the increase of gas velocity.

Fig. 4(b) shows the standard deviation of pressure fluctuations for a fluidized bed with a tube diameter of 100 mm. As the surface gas velocity increases, the pressure fluctuation shows an increase, then a decrease, and then an increase between 20.4 and 22.4 Pa, which is quite different from the standard deviation of pressure fluctuation for ordinary particle fluidization. When the gas velocity is low, the bed shows a trench flow phenomenon, *i.e*., a single large bubble passes through the bed, leading to an increase in the amplitude of pressure fluctuations. After the gas velocity increases, the agglomerates within the bed are compacted under the action of air pressure and its gravity, and the bed is de-fluidized as a whole, and the amplitude of pressure fluctuation becomes smaller at this time. When the gas velocity continues to increase, the bed splits into two parts, with the upper layer de-fluidized and the lower layer fully fluidized. The phenomenon of powder bridging appears, as shown in Fig. 5.

Under the gas pressure brought by the airflow, the upper part of the bed is lifted as a whole and does not enter the fluidization state, whereas the lower part of the bed enters the turbulent fluidization state within the limited space of the cone. This is caused by the higher interparticle forces due to the unique three-dimensional mesh structure of the carbon nanotube clusters, as shown in Fig. 6. Due to the high van der Waals forces between the particles, as well as the gravitational effect of the high bed surface and the compressive effect of the gas pressure below, the carbon nanotube clusters at the upper part of the bed surface easily clump together to form relatively tight aggregates. In the cylindrical cross-section at the upper part of the bed, the gas velocity is constant and low and cannot break through the carbon nanotube agglomerates, which causes the air pressure below the agglomerates to rise continuously and lift them as a whole. In the lower part of the bed, at the cone with a smaller inner diameter, where the gas velocity is several times higher than at the cylindrical cross-section, the carbon nanotube agglomerates here are broken by the high gas velocity. The broken small carbon nanotube agglomerates enter the turbulent fluidization state, causing the pressure fluctuation amplitude to appear suddenly in waves at this point. As the gas velocity continues to rise, the carbon nanotube agglomerates on the cylindrical cross-section of the fluidized bed are also lifted with the increase in air pressure below. After reaching the highest point and being broken up by the high gas velocity, the upper part of the bed falls back to the lower cone. At this point, the bed as a whole enters the particle fluidization state, and the pressure-fluctuation amplitude decreases. With the further increase of gas velocity, the bed as a whole successively enters the bubble fluidization and turbulent fluidization states, which makes the pressure fluctuation amplitude rise steadily.

Fig. 4(c) shows the pressure fluctuations inside the 300-mm-tube-diameter fluidized bed, which fluctuate between 12.4 and 14.0 Pa. The pressure-fluctuation amplitude decreases and then increases slowly with the increase of gas velocity. When the gas velocity is low, the sources of pressure fluctuation in the bed are mainly channel flow and large bubbles. As the gas velocity increases, the channels of channel flow in the bed are bridged and eliminated by gas pressure. The bed as a whole starts from particle fluidization and enters into bubble fluidization, turbulent

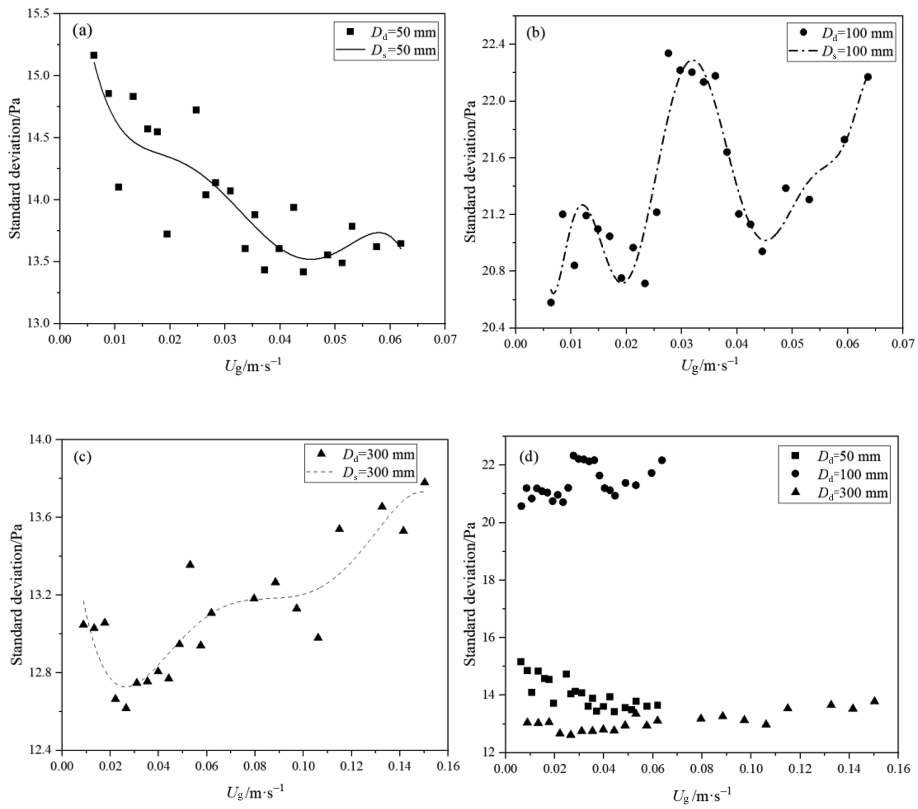

Fig. 4. Standard deviations of pressure fluctuation of distributor-less fluidized beds with different diameters: (a) 50 mm, (b) 100 mm, (c) 300 mm and (d) 50–300 mm.

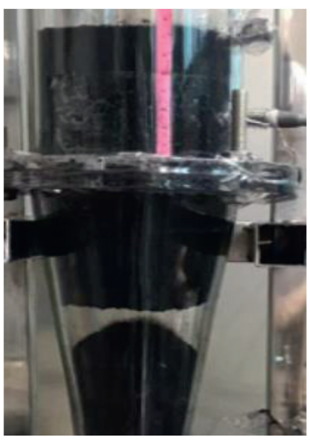

Fig. 5. Fluidization image of carbon nanotube agglomerates in 100-mm-bed-size fluidized bed at $U_g = 0.0318$ m·s^{-1}.

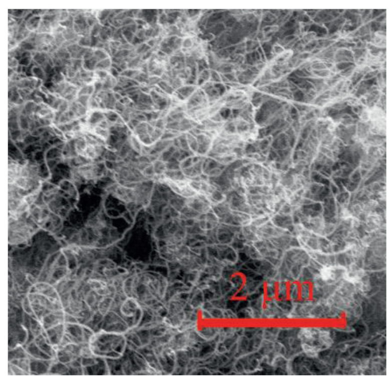

Fig. 6. Three-dimensional mesh structure of carbon nanotube clusters.

fluidization, and finally complete fluidization, successively. The amplitude of pressure fluctuation increases steadily. Fig. 4(d) shows the comprehensive comparison of the standard deviation of fluctuations of carbon nanotube clusters in the fluidized bed with three different tube diameters. It can be seen that the pressure fluctuations of carbon nanotube clusters in the 100-mm-diameter fluidized bed are much higher than those in the 50 and 300-mm-diameter fluidized beds, and the pressure fluctuations of carbon nanotube clusters in the 50-mm-diameter fluidized bed are slightly higher than those in the 300-mm-diameter fluidized bed. This is related to the upper and lower stratified bed morphology observed in the 100-mm-tube-diameter fluidized bed, where high-pressure fluctuations, inadequate fluidization, and high energy losses, as well as excessive gas velocities, make the gas residence time decrease and lower raw material utilization, which is not economically and environmentally efficient. This is also a phenomenon that needs to be avoided when designing and scaling-up fluidized beds.

4.2. Skewness and kurtosis of pressure fluctuations

The skewness indicates the degree of asymmetry of the probability density function. If the skewness is <0, the data are left--skewed with a long right tail; Conversely, if the skewness is >0, the data are right-skewed. Kurtosis is used to describe the relative peak of the probability density function [21]. Fig. 7 shows the effect of different bed diameters on the skewness and kurtosis of pressure fluctuations with increasing gas velocity. From Fig. 7(a), it can be seen that the fluidized bed with a diameter of 50 mm has the highest skewness, between 0.20 and 0.45, which fluctuates up and down with increasing gas velocity, whereas the skewness of the 300-mm-diameter fluidized bed is slightly lower, between 0.15 and 0.35, with a slight upward trend with the increase of gas velocity. The data distribution of these two beds is slightly right-skewed with pressure-fluctuation peaks and long tails on the right side of the distribution. The skewness of the 100-mm-diameter fluidized bed is very low, with constant positive values between 0 and 0.05, hardly varying with gas velocity, and the data are more evenly distributed around the mean value.

From Fig. 7(b), it can be seen that the kurtosis of the pressure-fluctuation data for the three beds always remains below 0.9. The kurtosis is the highest for the 50 and 300-mm-diameter fluidized beds, ranging from 0.15 to 0.9. The kurtosis distribution is larger for the 50-mm-diameter fluidized bed than for the 300-mm-diameter fluidized bed, and the peak pressure fluctuations are higher and sharper for these two fluidized beds. The kurtosis of the 100-mm-diameter fluidized bed was less than 0, between −0.105 and −0.60, and the peaks of pressure fluctuations in this bed were shorter and flatter. In general, all three beds have smooth pressure fluctuation peaks between −1.2 and 1.2.

The conclusions obtained from this experiment for fluidization experiments with three different bed diameters are in good agreement with the experimental results of our previous study [9]. This experiment shows that when carbon nanotube clusters are fluidized in a distributor-less conical fluidized bed, the wall effect decreases with increasing bed diameter.

4.3. Wavelet analysis of pressure-fluctuation signals

Fig. 8 shows the pressure fluctuation signals for three fluidized beds with diameters of 50, 100 and 300 mm, respectively. The data were measured at a gas velocity of 0.06 $m \cdot s^{-1}$ when the carbon nanotube clumps in the reactor were in a fully fluidized state. It can be seen that the original measured signals consist of multiple sequences of noise signals, and the amplitude and temporal behavior of the signals of the three beds are very similar, all belonging to the single-bubble mode. Among them, the pressure fluctuation frequency of the 300-mm bed is the lowest, which is only about half of the pressure-fluctuation frequency of the 100-mm bed, whereas the pressure fluctuation frequency of the 50-mm bed is the highest. It can be seen that the pressure-fluctuation frequency increases with decreasing bed diameter and shows a nonlinear trend, which indicates that the pressure-fluctuation frequency of the fluidized bed is related to the bed diameter.

The energy contribution share of carbon nanotube clusters within the conical fluidized bed of different diameters for each structure is detailed in Figs. 9–11. As shown in Figs. 9(a) and 10(a), the energy contribution of the 300-mm-diameter fluidized bed at the microscopic scale ranges from 50% to 75%, and the energy contribution at the mesoscopic scale ranges from 25% to 45%, and it fluctuates widely with gas velocity. The two scales, microscopic and mesoscopic, occupy 95% of the energy distribution, which is different from the results for the 50 and 100-mm-diameter fluidized beds. The microscopic scale occupies more than 95% of the energy distribution and does not fluctuate much with the gas velocity. This experiment validates Zhang's experiments [9] and proves that the bed size affects the energy distribution of the different structures of the fluidization process.

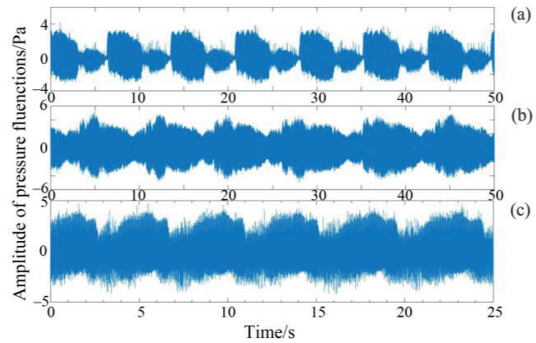

Fig. 8. Pressure-fluctuation signals at the same gas velocity for fluidized bed reactor diameters of (a) 50 mm, (b) 100 mm and (c) 300 mm, respectively.

Figs. 9(b), 10(b) and 11(b) show the similarities and differences in the energy structure distribution of carbon nanotube clusters in conical fluidized beds with 50 and 100-mm diameters. The fluidization behavior of carbon nanotube clusters in both 50 and 100-mm conical fluidized beds is dominated by the microstructure, *i.e.*, particle-to-particle collisions. This is because these two beds are smaller than 125 mm in diameter and are lab-scale fluidized beds, where the wall effect brings more influence. However, there are differences in the fluidization behavior of these two beds. The energy of the 100-mm-diameter fluidized bed is almost completely distributed in the microstructure, with only a slight attenuation at high gas velocities. This is related to the lap-bridge phenomenon, in which the upper layer of the carbon nanotube cluster bed is defluidized, and the lower layer is fully fluidized. The fluctuation of the mesoscopic energy distribution of carbon nanotube clusters in the 50-mm-diameter conical fluidized bed is higher than that in the 100-mm-diameter fluidized bed. The energy proportion of the macroscopic structure in the 50-mm-diameter conical fluidized bed is also the highest among the three beds types. This indicates that a small fraction of the energy of carbon nanotube clusters in

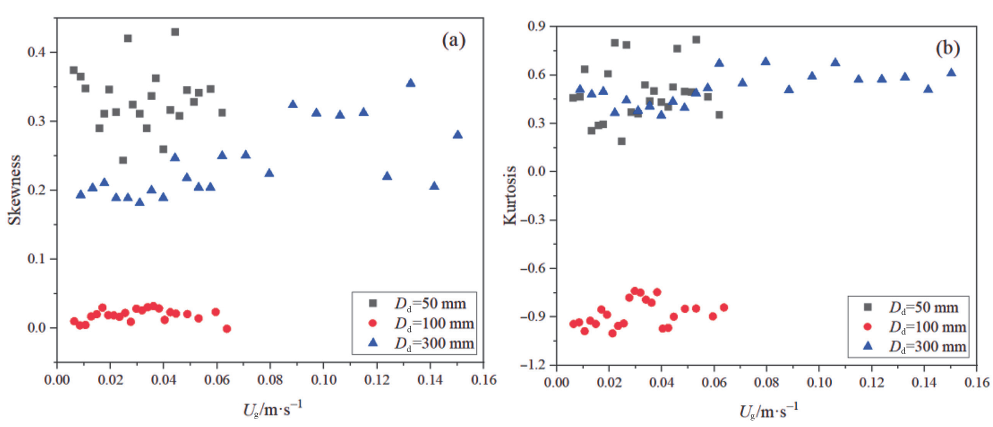

Fig. 7. Skewness and kurtosis of pressure fluctuations in different bed diameters ($D/H = 1:2, d_p = 0.35$ mm): (a) skewness and (b) kurtosis.

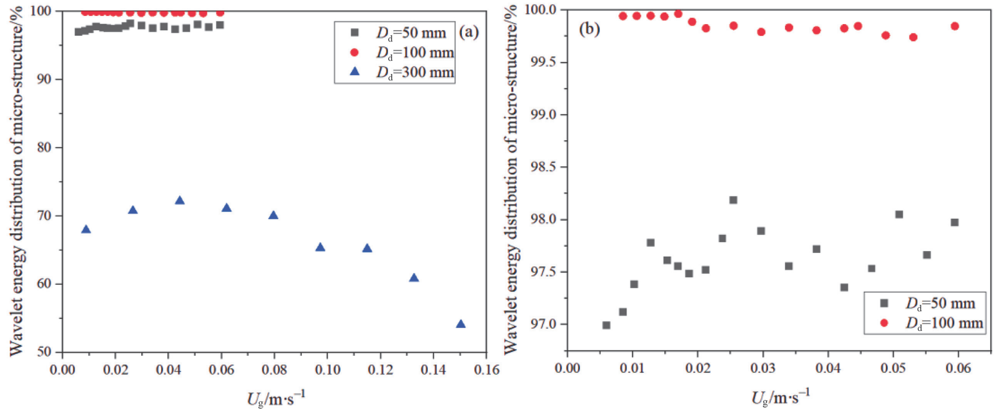

Fig. 9. Percentage energy contributions of microstructure at different fluidized bed diameters: (a) 50–300 mm and (b) 50–100 mm.

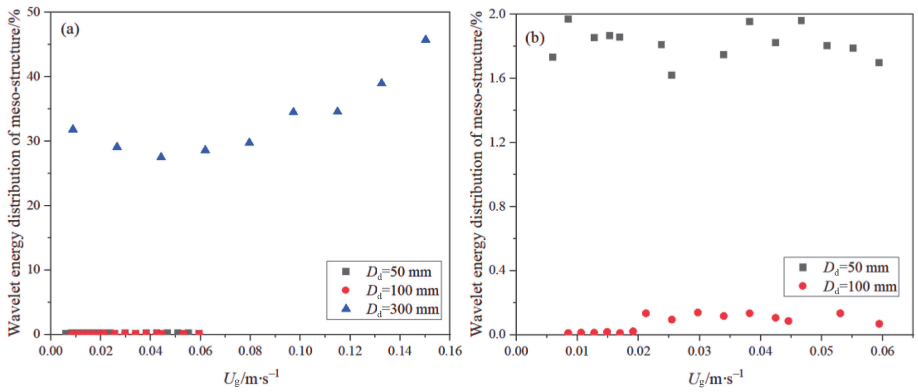

Fig. 10. Percentage energy contributions of mesostructure at different fluidized bed diameters: (a) 50–300 mm and (b) 50–100 mm.

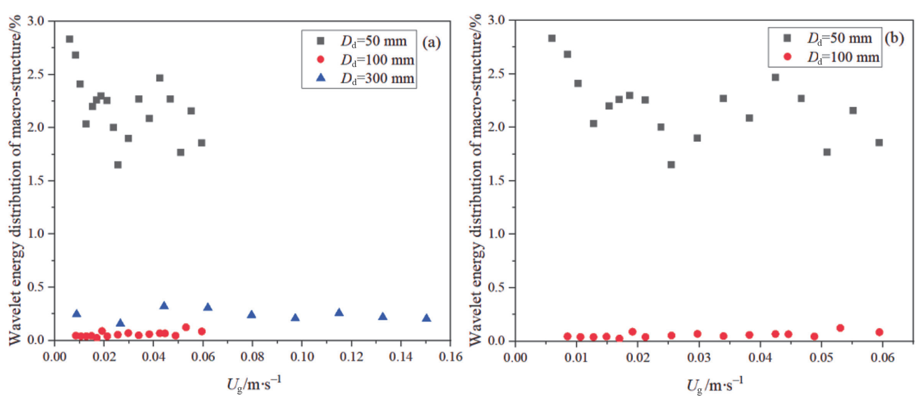

Fig. 11. Percentage energy contributions of macrostructure at different fluidized bed diameters: (a) 50–300 mm and (b) 50–100 mm.

the 50-mm-diameter conical fluidized bed is wasted on gas–gas and fluidized bed inner wall surface collisions.

As the diameter of the distributor-less conical fluidized bed expands step by step, the bubble eruption frequency gradually decreases, and the bubble size gradually increases. In the 100-mm bed diameter condition, the fluidized mass is weaker than that for 50-mm bed diameter due to the powder-bridging phenomenon, but after the bridging phenomenon disappears, the fluidized mass picks up again. The 300-mm-bed-diameter fluidized bed has partial energy loss during bubble movement and rupture.

5. Conclusions

In this work, the fluidization behavior and fluidization properties of carbon nanotube clusters in three distributor-less fluidized beds with 50, 100 and 300-mm diameters were investigated by mathematical methods such as time-series analysis and wavelet analysis. The conclusions of this study can be summarized as follows:

(1) In all three conical fluidized beds, the gas breaks through the center of the bed, which is caused by the distributor-less design.

(2) Carbon nanotube clusters in a conical fluidized bed with a diameter of 100 mm show a bridging phenomenon with the upper layer deliquescent and the lower layer completely fluidized. This phenomenon causes high-pressure fluctuation, insufficient fluidization, and high energy loss. Moreover, high gas velocity also makes the residence time of gas decrease, which reduces the utilization rate of raw materials.
(3) The pressure fluctuation frequencies of the carbon nanotube clusters in the three conical fluidized beds with different diameters were different. This indicates that the frequency of pressure fluctuation in a distributor-less conical fluidized bed is related to the bed diameter and that its trend is nonlinear.
(4) It was confirmed within a certain range that the bed size affects the multi-scale energy structure distribution of carbon nanotube clusters within a distributor-less conical fluidized bed.

Declaration of Interest

The authors declare that they have no known competing financial interests or personal relationships that could have appeared to influence the work reported in this paper.

Acknowledgements

This work was supported by the National Natural Science Foundation of China (52336003, 52206096, 52176076) and the Special Expert Project of Shandong Province Taishan Scholars Program (ts20190937).

Nomenclature

a	dilation factor
b	translation factor
D	diameter of fluidized bed
$D_j(t)$	the energy of the detail signal
d_p	equivalent diameter of CNTs, mm
E	the energy of a signal, Pa^2
E_A^J	the decomposed cumulative energy of level J approximation signals, Pa^2
E_D^j	the decomposed cumulative energy of different level j detail signals, Pa^2
g	gravity acceleration
H	static bed height, m
H_0	static initial bed height, m
J	desired decomposition level of multi-scale decomposition
j	wavelet decomposition level
K	kurtosis
N	total number of samples
n	total sampling point
S	skewness
U_g	superficial gas velocity, $m \cdot s^{-1}$
$W_f(a,b)$	wavelet coefficient
$X(t)$	the orthogonal wavelet level approximates the continuous signal
x	pressure fluctuation signals
$\overline{x}$	average pressure, Pa
$x(n)$	a series of time signals points
$x(t)$	raw time series signal
ε	particle porosity of CNTs, %
ρ_t	true density of CNTs, $g \cdot cm^{-3}$
σ	standard deviation, Pa
$\varphi_{a,b}^{*}(t)$	wavelet basis function

References

[1] L.S. Fan, Summary paper on fluidization and transport phenomena, *Powder Technol.* 88 (3) (1996) 245–253.
[2] F.J. Van Antwerpen, The origins of chemical engineering, in: W.F. Furter (Ed.), History of Chemical Engineering Washington (1980).
[3] B. Suleimenova, B. Aimbetov, D. Shah, E.J. Anthony, Y. Sarbassov, Attrition of high ash Ekibastuz coal in a bench scale fluidized bed rig under O_2/N_2 and O_2/CO_2 environments, *Fuel Process. Technol.* 216 (2021) 106775.
[4] Z.M. Yuan, Z. Huang, S.X. Ma, G.J. Zhao, H.R. Yang, G.X. Yue, Experimental investigation on the effect of superficial gas velocity on bubble dynamics properties of B particles in gas–solid fluidized bed reactor using digital image analysis technique, *Fuel* 348 (2023) 128617.
[5] S. Manzoor, J. Tatum, O.B. Wani, E.R. Bobicki, Comminution of carbon particles in a fluidized bed reactor: A review, *Miner. Eng.* 195 (2023) 108026.
[6] M. Seemann, Methanation of Biosyngas in a Fluidized Bed Reactor—Development of a One-step Synthesis Process, Featuring Simultaneous Methanation, Watergas Shift and Low Temperature Tar Reforming, PhD Thesis, ETH Zurich, 2006.
[7] J. Kopyscinski, T.J. Schildhauer, S.M.A. Biollaz, Production of synthetic natural gas (SNG) from coal and dry biomass—A technology review from 1950 to 2009, *Fuel* 89 (8) (2010) 1763–1783.
[8] J. Kopyscinski, T.J. Schildhauer, S.M.A. Biollaz, Employing catalyst fluidization to enable carbon management in the synthetic natural gas production from biomass, *Chem. Eng. Technol.* 32 (3) (2009) 343–347.
[9] T.L. Zhang, W.J. Bai, Q.P. Dong, D.M. Chu, Y.R. Yu, C. Yan, Y. Li, Y. He, Hydrodynamic analysis of carbon nanotube in pilot-scale distributor-less tapered fluidized bed, *Powder Technol.* 409 (2022) 117846.
[10] A. Baydin, F. Tay, J.C. Fan, M. Manjappa, W.L. Gao, J. Kono, Carbon nanotube devices for quantum technology, *Materials* 15 (4) (2022) 1535.
[11] K. Godlewska, M. Paszkiewicz, Reusable passive sampler with carbon nanotubes for monitoring contaminants in wastewater: Application, regeneration and reuse, *Chemosphere* 332 (2023) 138855.
[12] Y. Wang, W.Z. Yao, H.B. Huang, J. Huang, L. Li, X.H. Yu, Polypyrrole-derived carbon nanotubes for potential application in electrochemical detection of dopamine, *Solid State Sci.* 134 (2022) 107038.
[13] I.A. Khan, A. Rai, J.P. Keshari, M. Nizamuddin, S. Nayak, D. Sharma, Design, simulation and comparative analysis of carbon nanotube based energy efficient priority encoders for nanoelectronic applications, *E Prime Adv. Electr. Eng. Electron. Energy* 4 (2023) 100138.
[14] Z.W. Chen, J.G. Zhao, J.F. Cao, Y.Y. Zhao, J.Q. Huang, Z.S. Zheng, W.J. Li, S. Jiang, J. Qiao, B.Y. Xing, J. Zhang, Opportunities for graphene, single-walled and multi-walled carbon nanotube applications in agriculture: A review, *Crop Des* 1 (1) (2022) 100006.
[15] B. Tynan, Y. Zhou, S.A. Brown, L.M. Dai, A.N. Rider, C.H. Wang, Structural supercapacitor electrodes for energy storage by electroless deposition of MnO_2 on carbon nanotube mats, *Compos. Sci. Technol.* 238 (2023) 110016.
[16] F. Wei, Q. Zhang, W.Z. Qian, H. Yu, Y. Wang, G.H. Luo, G.H. Xu, D.Z. Wang, The mass production of carbon nanotubes using a nano-agglomerate fluidized bed reactor: A multiscale space–time analysis, *Powder Technol.* 183 (1) (2008) 10–20.
[17] W.J. Bai, D.M. Chu, Y. He, Fluidization dynamic characteristics of carbon nanotube particles in a tapered fluidized bed, *Chin. J. Chem. Eng.* 44 (2022) 321–331.
[18] W.J. Bai, D.M. Chu, F. Wang, Y. He, Research on fluidization performance of different tapered fluidized bed reactors for fluidizing carbon nanotubes, *Ind. Eng. Chem. Res.* 59 (25) (2020) 11893–11904.
[19] J.W. Chew, W.C.Q. LaMarche, R.A. Cocco, 100 years of scaling up fluidized bed and circulating fluidized bed reactors, *Powder Technol.* 409 (2022) 117813.
[20] K. Dasgupta, J.B. Joshi, H. Singh, S. Banerjee, Fluidized bed synthesis of carbon nanotubes: Reaction mechanism, rate controlling step and overall rate of reaction, *AIChE J.* 60 (8) (2014) 2882–2892.
[21] S. Fang, Y.D. Wei, L. Fu, G. Tian, H.B. Qu, Time-series analysis of the characteristic pressure fluctuations in a conical fluidized bed with negative pressure, *Chin. J. Chem. Eng.* 32 (2021) 87–99.
[22] C. Sheng, C.L. Duan, Y.M. Zhao, L. Dong, Z.F. Luo, Analysis and evaluation on pressure fluctuations in air dense medium fluidized bed, *Int. J. Min. Sci. Technol.* 28 (3) (2018) 461–467.
[23] J.R. van Ommen, R.J. de Korte, C.M. van den Bleek, Rapid detection of defluidization using the standard deviation of pressure fluctuations, *Chem. Eng. Process* 43 (10) (2004) 1329–1335.
[24] C. Sobrino, S. Sánchez-Delgado, N. García-Hernando, M. de Vega, Standard deviation of absolute and differential pressure fluctuations in fluidized beds of group B particles, *Chem. Eng. Res. Des.* 86 (11) (2008) 1236–1242.
[25] S.M. Okhovat-Alavian, J. Behin, N. Mostoufi, Investigating the flow structures in semi-cylindrical bubbling fluidized bed using pressure fluctuation signals, *Adv. Powder Technol.* 30 (6) (2019) 1247–1256.
[26] Z.Z. Ma, H.F. Ma, W.X. Qian, H.T. Zhang, Q.W. Sun, W.Y. Ying, Bubble behaviors in a dense gas–solids fluidized bed: Analysis of pressure fluctuation, *Chem. Eng. Technol.* 45 (9) (2022) 1675–1682.
[27] F. Johnsson, R.C. Zijerveld, J.C. Schouten, C.M. van den Bleek, B. Leckner, Characterization of fluidization regimes by time-series analysis of pressure fluctuations, *Int. J. Multiphas. Flow* 26 (4) (2000) 663–715.
[28] Y.D. Zhang, Y.M. Zhao, L. Dong, C.L. Duan, E.H. Zhou, J.Y. Lu, B. Zhang, X.L. Yang, Flow pattern transition characteristics in vibrated gas–solid fluidized bed of Geldart B magnetite powder using pressure drop signals analysis, *Powder Technol.* 327 (2018) 358–367.

[29] Y.D. Zhang, X.Y. Zhang, Y.M. Zhao, G.N. Lv, X.L. Yang, Z.M. Wang, C.L. Duan, L. Dong, Bubble growth obtained from pressure fluctuation in vibration separation fluidized bed using wavelet analysis, *Adv. Powder Technol.* 31 (8) (2020) 3287–3296.
[30] M. Bassenne, P. Moin, J. Urzay, Wavelet multiresolution analysis of particle-laden turbulence, *Phys. Rev. Fluids* 3 (8) (2018) 084304.
[31] B. Li, X.F. Chen, Wavelet-based numerical analysis: A review and classification, *Finite Elem. Anal. Des.* 81 (2014) 14–31.
[32] G.P. Wu, Y. He, L.A. Luo, W. Chen, Dynamic characterizations of gas–solid flow in a novel multistage fluidized bed *via* nonlinear analyses, *Chem. Eng. J.* 359 (2019) 1013–1023.
[33] S.G. Mallat, A theory for multiresolution signal decomposition: The wavelet representation, *IEEE Trans. Pattern Anal. Mach. Intell.* 11 (7) (1989) 674–693.
[34] W.J. Bai, D.M. Chu, Y. He, The minimum fluidization velocity and dynamic characteristics of agglomerated carbon nanotube in a tapered fluidized bed at elevated temperature, *Chem. Eng. Res. Des.* 168 (2021) 239–253.
[35] G.P. Wu, Y. He, L.A. Luo, W. Chen, Dynamic characterizations of gas–solid flow in a novel multistage fluidized bed *via* nonlinear analyses, *Chem. Eng. J.* 359 (2019) 1013–1023.
[36] H.J. Sun, C.B. Hu, Y.H. Xu, Pressure fluctuations analysis on the powder fluidization performance at different pressure, *Int. J. Multiphas. Flow* 116 (2019) 176–184.
[37] C. Sheng, C.L. Duan, Y.M. Zhao, L.A. Dong, Z.F. Luo, Analysis and evaluation on pressure fluctuations in air dense medium fluidized bed, *Int. J. Min. Sci. Technol.* 28 (3) (2018) 461–467.